THE REPUBLIC OF TURKEY
BAHCESEHIR UNIVERSITY

ALL IN FOCUS IMAGES

Master's Thesis

CANFEDA KARABULUT

ISTANBUL, 2015

THE REPUBLIC OF TURKEY
BAHCESEHIR UNIVERSITY

GRADUATE SCHOOL OF NATURAL AND APPLIED SCIENCES
COMPUTER ENGINEERING

ALL IN FOCUS IMAGES

Master's Thesis

CANFEDA KARABULUT

Thesis Supervisor: PH. D. TARKAN AYDIN

ISTANBUL, 2015

THE REPUBLIC OF TURKEY
BAHCESEHIR UNIVERSITY

GRADUATE SCHOOL OF NATURAL AND APPLIED SCIENCES
COMPUTER ENGINEERING

Name of the thesis: All In Focus Images
Name/Last Name of the Student: Canfeda Karabulut
Date of the Defense of Thesis: 02.09.2015

The thesis has been approved by the Graduate School of Natural and Applied Sciences.

Assoc. Prof. Nafiz ARICA
Graduate School Director
Signature

I certify that this thesis meets all the requirements as a thesis for the degree of Master of Science.

Ph. D. Tarkan AYDIN
Program Coordinator
Signature

This is to certify that we have read this thesis and we find it fully adequate in scope, quality and content, as a thesis for the degree of Master of Science.

Examining Comittee Members	Signature
Thesis Supervisor Ph. D. Tarkan AYDIN	----------
Thesis Co-supervisor Ph. D. Cemal Okan ŞAKAR	----------
Member Assoc. Prof. Ali SIRMA	----------

ABSTRACT

ALL IN FOCUS IMAGES

Canfeda Karabulut

Computer Engineering Graduate Program

Thesis Supervisor: Ph. D. Tarkan Aydın

September 2015, 58 pages

The reason of the limited depth of field in optic lenses used in the camera system, out of focused areas are blurry in the image and image does not give exact information about scene. In order to learn exact information about objects in the scene, an image where all objects are in focused is acquired. This image is All In Focus Image. For this acquisition, focused areas in the image are found by using several images from same scene which are captured with different focus settings. Then, these focused areas are combined together to get All In Focus image.

In this thesis, thirty five different focus measure operators were used to detect focused areas. Detected focused areas combined together to get an All In Focus Image where all objects are in focus. Each result image which was acquired with focus measure operators was compared with a reference image which was taken with small aperture size of a camera. Images were compared with five different quality metrics. According to the result of the metrics, focus measure operators which provide to generate the most and the least informative All In Focus Image about scene were found.

Keywords: All In Focus Image, Image Stacking, Omni Focus Image, Focus Measure Operators

ÖZET

ODAKLANILMIŞ GÖRÜNTÜ ELDE ETME

Canfeda Karabulut

Bilgisayar Mühendisliği Yüksek Lisans Programı

Tez Danışmanı: Yrd. Doç. Dr. Tarkan Aydın

Eylül 2015, 58 sayfa

Kameralarda bulunan lensler sınırlı alan derinliğine sahip olduğu için odaklanılmamış alanlar imgelerde bulanıktır ve görüntüler sahne hakkında tam bilgi vermez. Sahnedeki tüm nesneler hakkında tam bilgi almak için sahnedeki tüm nesnelerin odaklanılmış tek bir görüntüsü elde edilir. Bunun için sahnenin farklı odak değerleriyle çekilmiş görüntüleri alınarak odaklanılmış alanlar bulunur. Daha sonra bu odaklanılmış alanlar birleştirilerek sahnedeki tüm nesnelerin odaklanılmış görüntüsüne ulaşılır.

Bu tezde, sahnede bulunan tüm nesnelerin odaklanılmış görüntüsüne ulaşmak için literatürde bulunan otuz beş farklı odak ölçütü kullanılarak odaklanılmış bölgeler bulunmuş ve bu bölgeler birleştirilmiştir. Her bir odak ölçütüne göre çıkan sonuçlar sahnenin en net görüntüsüyle (referans görüntüsü) kıyaslanarak, sahne hakkında en fazla bilgi verenle en az bilgi veren odak ölçütleri bulunmuştur. Görüntüler beş farklı metrikle kıyaslanmıştır.

Anahtar Kelimeler: Odaklanılmış Alanlar, Odak Ölçütleri, Odak Ölçütleri Kıyaslama

CONTENTS

TABLES viii

FIGURES ix

ABBREVIATION xii

SYMBOLS xiv

1. INTRODUCTION 1

2. ALL IN FOCUS IMAGES 5

2.1 IMAGE FORMATION 5

2.2 ALL IN FOCUS IMAGES METHOD 6

2.3 FOCUS MEASURE OPERATORS 8

2.3.1 Variance Focus Measure (GLVA) 9

2.3.2 Grey Level Local Variance (GLLV) 10

2.3.3 Normalized Grey Level Variance (GLVN) 10

2.3.4 Modified Grey Level Variance (GLVM) 10

2.3.5 Mean Method Focus Measure (HELM) 10

2.3.6 Curvature Focus Measure (CURV) 11

2.3.7 Energy Gradient (GRAE) 11

2.3.8 Tresholded Gradient (GRAT) 11

2.3.9 Squared Gradient (GRAS) 12

2.3.10 Tenengrad (TENG) 12

2.3.11 Tenengrad Variance (TENV) 12

2.3.12 Vollath's Correlation (VOLA) 13

2.3.13 Vollath's Standard Deviation (VOLS) 13

2.3.14 Laplacian 13

2.3.15 The Energy Laplacian 14

2.3.16 Sum Modified Laplacian (LAPM) 14

2.3.17 Variance of Laplacian(LAPV) 14

2.3.18 Diagonal Laplacian (LAPD) 15

2.3.19 3D Laplacian 15

2.3.20 Laplacian in 3D Window (LAP3) 15

2.3.21 Histogram Entropy (HISE) 15

2.3.22 Histogram Range (HISR) 16

2.3.23 Steerable Filter (SFIL) 16

2.3.24 Spatial Frequency (SFRQ) 16

2.3.25 Image Moment 17

2.3.26 Chebyshev Moments Based Focus Measure Operator (CHEB) 17

2.3.27 Absolute Central Moment (ACMO) 18

2.3.28 Brenner's Focus Measure (BREN) 18

2.3.29 Image Contrast (CONT) 18

2.3.30 Eigenvalues Based Focus Measure Operator (EIGV) 19

2.3.31 Gausian Derivative Focus Measure Operator (GDER) 19

2.3.32 Susan Operator 19

2.3.33 Sum of Wavelet Coefficients (WAVS) 20

2.3.34 Ratio of Wavelet Coefficients (WAVR) 20

2.3.35 Variance of Wavelet Coefficients (WAVV) 20

2.3.36 The Discrete Cosine Transform (DCT) 21

2.3.37 DCT Energy Ratio (DCTE) 22

2.3.38 DCT Reduced Energy Ratio (DCTR) 22

2.3.39 Modified DCT (DCTM) 23

2.3.40 Energy of S Transform 23

2.3.41 Bipolar Image Filter 23

2.4 IMAGE QUALITY METRICS 24

3. EXPERIMENTS 27

3.1 TEST ON REAL DATA AND SYNTHETIC DATA 27

3.2 METHOD 27

3.3 COMPARISION OF FOCUS MEASURE OPERATORS 28

3.3.1 Deer Images 28

3.3.2 Mozart Images 35

3.3.3 Venus Images 41

3.4 EVALUATING THE WINDOW SIZE FOR MOZART IMAGE 46

4. CONCLUSION 50

REFERENCE 52

TABLES

Table 3.1: Best results according to quality metrics for Deer Sequence 28

Table 3.2: Poor result according to quality metrics for Deer Sequence..... 30

Table 3.3: Focus measure and Time for Deer Sequence..... 34

Table 3.4: Best results according to quality metrics for Mozart Sequence..... 35

Table 3.5: Poor result according to quality metrics for Mozart Sequence..... 36

Table 3.6: Focus measure and Time for Mozart Sequence..... 40

Table 3.7: Best result according to quality metrics for Venus Sequence..... 41

Table 3.8: Poor Result According to Quality Metrics for Venus Sequence 41

Table 3.9: Focus measure and time for Venus Sequence..... 45

Table 3.10: Best results according to Normalized Cross Correlation..... 47

Table 3.11: Poor results according to Normalized Cross Correlation 47

Table 3.12: Best results according to SSIM..... 48

Table 3.13: Poor results according to SSIM 48

FIGURES

Figure 2.1: Principal of Image Formation Geometry 5

Figure 3.1: Image Comparision 29

Figure 3.2: Image which is acquired with DCTE 29

Figure 3.3: Image which is acquired with WAVR 30

Figure 3.4: The maximum SSIM value order for Deer Sequence 31

Figure 3.5: The minimum SSIM value order for Deer Sequence 31

Figure 3.6: The maximum PSNR value order for Deer Sequence 31

Figure 3.7: The minimum PSNR value order for Deer Sequence 32

Figure 3.8: The maximum Normalized Cross Correlation value order for Deer Sequence 32

Figure 3.9: The minimum Normalized Cross Correlation value order for Deer Sequence 32

Figure 3.10: The maximum Mean Square value order for Deer Sequence 33

Figure 3.11: The minimum Mean Square Error value order for Deer Sequence 33

Figure 3.12: The maximum Normalized Absolute Error value order for Deer Sequence 33

Figure 3.13: The minimum Normalized Absolute Error value order for Deer Sequence 33

Figure 3.14: The maximum elapsed time order for Deer Sequence 34

Figure 3.15: The minimum elapsed time order for Deer Sequence 34

Figure 3.16: Image which is acquired with CURV 36

Figure 3.17: The maximum SSIM value order for Mozart Sequence 37

Figure 3.18: The minimum SSIM value order for Mozart Sequence 37

Figure 3.19: The maximum PSNR value order for Mozart Sequence 37

Figure 3.20: The minimum PSNR value order for Mozart Sequence 37
Figure 3.21: The maximum Normalized Cross Correlation value order for Mozart Sequence 38
Figure 3.22: The minimum Normalized Cross Correlation order for Mozart Sequence 38
Figure 3.23: The maximum Mean Square Error value order for Mozart Sequence 38
Figure 3.24: The minimum Mean Square Error value order for Mozart Sequence 39
Figure 3.25: The maximum Normalized Absolute Error value order for Mozart Sequence 39
Figure 3.26: The minimum Normalized Absolute Error value order for Mozart Sequence 39
Figure 3.27: The maximum elapsed time order for Mozart Sequence 40
Figure 3.28: The minimum elapsed time order for Mozart Sequence 40
Figure 3.29: The maximum SSIM value order for Venus Sequence 42
Figure 3.30: The minimum SSIM value order for Venus Sequence 42
Figure 3.31: The maximum PSNR value order for Venus Sequence 42
Figure 3.32: The minimum PSNR value order for Venus Sequence 42
Figure 3.33: The maximum Normalized Cross Correlation value order for Venus Sequence 43
Figure 3.34: The minimum Normalized Cross Correlation value order for Venus Sequence 43
Figure 3.35: The maximum Mean Square value order for Venus Sequence 43
Figure 3.36: The minimum Mean Square Error value order for Venus Sequence 44

Figure 3.37: The maximum Normalized Absolute Error value order for Venus Sequence.....44
Figure 3.38: The minimum Normalized Absolute Error value order for Venus Sequence.....44
Figure 3.39: The maximum elapsed time order for Venus Sequence.....45
Figure 3.40: The minimum elapsed time order for Venus Sequence.....45
Figure 3.41: Images acquired with CHEB using different window sizes 48

ABBREVIATION

ACMO	:	Absolute Central Moment
AIF	:	All In Focus
BREN	:	Brenner's
CHEB	:	Chebyshev Moments-based
CONT	:	Image Contrast
CURV	:	Image Curvature
DCTE	:	DCT Energy Ratio
DCTM	:	DCT Modified
DCTR	:	DCT Reduced Energy Ratio
DOF	:	Depth Of Field
EIGV	:	Eigenvalues-based
FM	:	Focus Measure
GDER	:	Gaussian Derivative
GLLV	:	Graylevel Local Variance
GLVA	:	Graylevel Variance
GLVM	:	Modified Graylevel Variance
GLVN	:	Normalized Graylevel Variance
GRAE	:	Energy of Gradient
GRAS	:	Squared Gradient
GRAT	:	Thresholded Gradient
GRA3	:	3D Laplacian
HELM	:	Helmli's Mean Method
HISE	:	Histogram Entropy
HISR	:	Histogram Range
LAPD	:	Diagonal Laplacian
LAPE	:	Energy of Laplacian
LAPM	:	Modified Laplacian
LAPV	:	Variance of Laplacian
LAP3	:	Laplacian in 3D Window
SFIL	:	Steerable Filters

SFRQ : Spatial Frequency

TENG : Tenengrad

TENV : Tenengrad Variance

VOLA : Vollath's Correlation

VOLS : Vollath's Standard Deviation

WAVR : Ratio of Wavelet Coefficients

WAVS : Sum of Wavelet Coefficients

WAVV : Variance of Wavelet Coefficients

SYMBOLS

Focus Measure Operator	:	F
Image	:	I
Image Stack	:	I_s

1. INTRODUCTION

An image gives information about scene where the image was captured. However, it may not give every detail about scene. Forefront objects may be sharpest than background objects in the image and give more information about scene objects, but the other objects in the image may not be sharp as forefront objects in the image and they do not give information about objects in the scene. Examples can be diversified. The reason of this situation is limited depth of field.

Optical lenses in digital camera suffer from the narrow depth of field, this problem decreases the image quality because blurry areas occur in the image and these areas do not give exact information about captured scene. When an object at the certain distance is focused, other objects at the same distance with focused object are seen sharp. Despite of this, objects at different distance from focus length are out of focus and they are seen blurry. The distance between nearest and furthest objects which are displayed acceptable sharpness is called depth of field (Aslantaş et al. 2013).

The depth of field depend on the magnification and aperture size of imaging system (Nayar and Nakagawa 1994). Aperture is a hole and it provides lights to pass through. Rays coming from a light source first hit an object and reflect, then they pass through aperture of a camera and fall into an image plane. This is the simplified explanation of image formation. Aperture size has an impact on transmitted lights and works like pupils. Therefore, reducing or increasing aperture size affects depth of field. If the aperture size decreases, the depth of field will increase. Reduction of aperture size causes diffraction effect which reduces the image sharpness. Therefore, reduction of the aperture size is not efficient to acquire image (Aslantas and Pham 2007). Magnification is also affect depth of field. Magnification is the enlarging process. When sensing plane of the camera which has a fixed focal length is moved along to optical axis, focused distance of the lens will vary. This change is the focus magnification. Changes in focus settings create magnification variations. These variations cause problems for some vision techniques like depth from defocus and All In Focus. In order to compensate focus magnification effects in focus ranging, two approaches have suggested. These are

constant image magnification, (Darrell and Wohn 1988) and large evaluation window to completely encompass the features being ranged, (Krotkov 1987).

In order to compensate depth of field, several images with different focus settings from the same scene are taken and combined together into an image. This method is called All in Focus Image Acquisition. The main goal of All In Focus Image Acquisition Techniques is to combine relevant information from the two or more images to get a frame where all objects are in focus. This single frame which is generated by using these methods has more precise information of the scene. These methods provide to enhance the image quality and information. Proposed algorithms for computation of the AIF image split into four categories. These are spatial frequency based methods, image pyramids, defocus modelling and wavelet transform, (Pertuz et al. 2013). Spatial frequency base methods use a sharpness measure or focus measure to determine pixels which have higher information content in each frame, (Tian and Chen 2010). Image pyramids base methods apply a multiscale decomposition of the image to determine pixels or areas which have higher information content at different scale (Antunes et al.2005; Zhang and Blum 1999). In defocus modelling, a known spread function model is used to recover AIF image and then a filter is used (Subbarao and Choi 1995; Kodama et al. 2007; Aguet et al. 2008). Wavelet transform base methods perform a wavelet decomposition of the focus sequence. Then wavelet coefficients are chosen according to some criterions. After the selection of coefficients, merging process is carried out in the wavelet domain (Tian and Chen 2010; Forster et al. 2004).

Before merging to get All In Focus Image, it is require to find best focused pixels or areas. Focused points are sharp and have high frequency image content. Therefore, sharpness of a pixel is evaluated by using focus measure operators which take a local neighborhood and compute the sharpness of the chosen center pixel. In order to find these pixels, different focus measure operators were proposed in the literature. Focus measure operators could be classified into six classes (Pertuz et al. 2012). Gradient-based operators are computed with the gradient or first derivative of the image. This kind of operators are based on the principle that focused images have more sharp edges than blurry images. Laplacian-based operators are computed with the second derivative

or Laplacian. This type also considers the amount of edges in the image. Wavelet based operators are based on the discrete wavelet transform to describe the frequency and spatial content of images. Statistics based operators are computed with using image statistics as texture descriptors. DCT based operators are computed with the cosine transformation and based on the frequency content in the image. Miscellaneous operators are the other operators which do not belong previous class.

After acquiring All In Focus Images, assesment necessity of computed results arises. This assesment is based on the comparision between two images. One of them is the AIF image which was acquired by focus measure operators. The other one is the reference image which was captured with small aperture size of a camera. This comparision performs with image quality metrics. Image quality measures could be grouped into six families according to their properties (Avcıbas et al. 2002; Al-Najjar and Chen 2012). Pixel difference based measures are quality metrics which consider difference between two images. These measures are easy to evaluate like PSNR, MSE. Correlation based measures like Normalized Cross Correlation are another type of quality metrics which consider correlation of pixels to reveal image quality. Edge based measures like Edge Stability Mesuare are also quality metrics which are based on the asumption that edges have important role in the image. Spectral distance based quality measures are computed with Discrete Fourier Transform. Context based quality measures are based on the asumption that the neighborhood information of pixels is important and any loss of contextual information could be considered for image quality metrics. Human visual system based measures are quality metrics which consider contrast, color and frequency change.

In this study, All In Focus Images were acquired by following two processes. In the first place, Focus measure operators were computed with using images of a sequence which were captured with different focus settings from a scene to determine high frequency content. For this process, tests were performed on two kind of datas which are real data and synthetic data. Real focus sequence of 27 images of 510 x 600 pixels (Mozart Sequence) and 14 images of 614 x 819 pixels (Deer Sequence) were used as a real data. Each image of a sequence was captured with different focus settings from same scene.

Synthetic data was generated with Iris filter from real all focus image. There are 32 images of 383 x 434 pixels in this focus sequence (Venus Image). Real all focused images (referenced images) were captured with the smallest aperture size for three scenes. Thirty five different focus measure operators in the litarature were used for this operation to find sharp area. After this process, focused area combined together to get a new frame where all objects are focused. Different focus measure operators produced different results. In order to determine which FM produced better result, each result image which was acquired with focus measure operators was compared with a reference image which was taken with small aperture size of a camera. Five different quality metrics were used. These metrics are Structural Similarity Index (SSIM), Peak Signal-to-Noise Ratio (PSNR), Normalized Cross Correlation, Mean Square Error, Normalized Absolute Error and they were selected among most widely used metrics. According to the result of these metrics, focus measure operators which provide to generate the most and the least informative All In Focus Image about scene were found. This study contains the comparision of different methods on All In Focus Image.

In this thesis, sections splited into these parts. In section 2, Accusition of the All In Focus Image and methods used in the literature were explained. Quality image metrics which provide to compare the results of FM operators also described in this part. In section 3, this section is experiment part, explained focus measure opertors which provide to detect focused area performed and compared each other with respect to their AIF result. In section 4, this is conclusion part of the study, findings were interpreted.

2. ALL IN FOCUS IMAGES

2D images which are taken with an open aperture lens have blurry and sharp areas. The limited depth of field of lenses used in cameras is the reason of blurriness which is correspond to distance in image which is acquired by that kind of camera. The focus area is the exception of this. The other words, scene points without the depth of field of the camera are blurry, while the other points are focused. It can be said that the captured images have little information about scene because of the depth of field which influence the quality and the amount of information which is retrieved from captured images.

Using shallow depth of field system makes the objects in focus plane closer. However, it makes the other objects at different depths from camera blurry if they are distant from the focus plane. In order to compensate for this problem, some methods are proposed to obtain All In Focus images which contain that all visible objects are focused (Kodama et al. 1996, Tsubaki et al. 2001, Antunes et al. 2005, Li and Yang 2008, Pertuz et al. 2013).

2.1 IMAGE FORMATION

This part is about image formation which is obtained by using ideal lenses. The simplest camera model is in Figure 2.1:

Figure 2.1: Principal of Image Formation Geometry

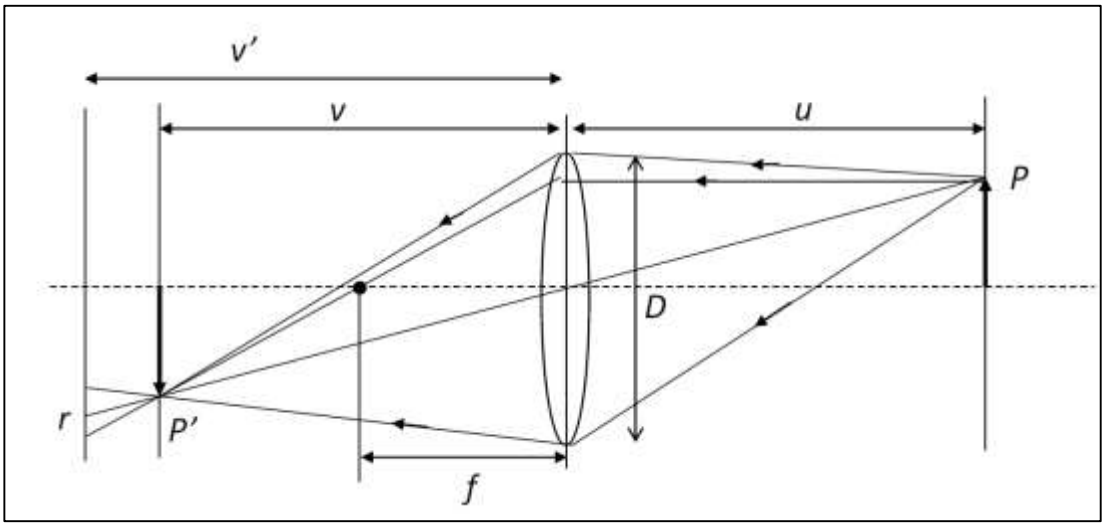

Source: Tarkan Aydin, (2011). Cifte ag metoduyla stereo, odak ve bulanıklık bilgisini kullanarak resimlerden derinlik çıkarımı.

In Figure 2.1, u is the object distance, f is focal length, v is projected distance, P is object, P' is projection, D is apareture.

In Figure 2.1, optic system contains a lens and a plane which are parallel each other. Image plane is composed of sensors which are capable of measuring the amount of light on image plane. Function of the lens used in the system leads the incoming light on the lens to specific direction. According to ideal lens rule, all rays arising from point source where is u distance away from lens must provide following condition to be collected on image plane where is v distance away from lens. (Born and Wolf 1965, Aydin 2011)

$$\frac{1}{u}+\frac{1}{v}=\frac{1}{f} \tag{2.1}$$

where f is known focal length. An area on focus is a plane which is parallel to image plane for ideal lens. It means that any scene point on the focused plane has an image on image plane. This image is also a point. It is called focused for the regions of these points and image fields which correspond to these points contain the sharpest image. When image plane shifts to v', focused plane will change. For this resaon, rays arising from any point where is not in new focused plane fall into a circle on image plane. This circle is called blur circle. r is the radius of the blur circle and it can be calculated with simple geometric operation. Radius of this circle depends on u, v, f and focal aparture D and it is found:

$$\mathrm{r}=\frac{(\mathrm{v}'-\mathrm{v})\mathrm{D}}{\mathrm{v}} \tag{2.2}$$

2.2 ALL IN FOCUS IMAGES METHOD

All In Focus Image methods provide to obtain an image where all objects are focused with using images from a sequence of different focus setting images which were captured from the same scene. In All In Focus, there are N different images of each scene point. The main aim of All In Focused Image is to find fully focused images from

scene points with the assumption of the same pixel coordiantion in each image which is a member of a sequence. The sequence of images are the combination of N different views of any point of a scene. Therefore, known focus adjustments of these images are found. Equation (2.1) illustrates the computation of distance of scene point corresponding to focused image point whose focus setting has known. The functions for measuring focus level of image pixels are used to find the best focused image of scene points. These functions are called Focus Measure Operator. After computation of the focus level, maximum focus measure positions are determined, pixels in those positions are taken to acquire All In Focus image:

$$I = I_s(D) \tag{2.3}$$

where I_s is the image stack and D is depth of the scene. I is referred to the All In Focus image.

In literature, AIF image acquisition method can be splitted into four main categories: these methods are based on the spatial frequency, image pyramids, defocus modeling, and wavelet transforms.

Most of the All In Focus methods are based on the following energy maximization scheme. (Pertuz et al. 2013, Aguet et al. 2008). Defocus modelling based method is the exception of this scheme.

i. $I_k(x,y)$ is an image stack which is obtained in spatial coordinates (x,y) and k is the frame number. Each I_k is an image which is taken at a certain focus distance.
ii. Either a high pass criterion or focus measurements is applied to each frame of the image stack.
iii. An index map is generated by the selection of the index which has the largest frequency or focus measeure for the each (x,y) position.
iv. Previous index map is exploited to generate the All In Focus image. In pyramid based or wavelet based methods usually require an inverse transformation to get All In Focus image.

The disadvantage of this scheme is the existence of noise, focus measure maximization add noise to result too. In order to compansate this problem, Pertuz et al. (2013) proposed an approach to combine the different frames of the focus sequence to acquire All In Focus Images. They developed noise robust algorithm. In this approach, they tried to reduce noise while preserving image features.

In section 2.3, focus measure operators which are used to acquire AIF Image are explained.

2.3 FOCUS MEASURE OPERATORS

Focus measure operators provide to detect best focused area. In order to detect, focus measure operators exploit the geometric analysis of image formation. According to the geometric analysis of image formation of Nayar and Nakagawa (1994), the bluriness is the process of the low pass filtering. In other words, bluriness degree is inversely proportional to the amount of high frequency content in an image. For this reason, focus measure operators which are used to find focused area in an image must be sensitive to high frequency image content and they require to produce the highest value in fully focused area. Therefore, many focus measure operators use functions which can measure the amount of high frequency content in images.

Ideal Focus Measure Operators must have these properties:

i. High values should be produced against high frequency variables in image brightness values. It means that focus measure operators should get high value for the specific scene point which is fully focused.
ii. Image should be independent from its content.
iii. It should be single mode. It means that the operator should have only one maximum point which must be correspond to focus situation where the image is focused.
iv. It should be monotonic function. Both sides of the functions' maximum point should be monotonic. It means that focus measure operator should decrease where the amount of bluriness increases.

In literature, various functions which are described in the spatial domain or frequency domain are used as a focus measure operator. Spatial based operators usually exploit high pass filter. Frequency based operators usually measure total energy in frequency distribution or calculate the ratio between high frequency components and low frequency components.

In this part, operators in the literature that are used as a focus measure are explained. The pixel value in the (x_0, y_0) position of a given I image is $I(x_0,y_0)$ and F is the focus measure value for this pixel value. $\Omega(x_0,y_0)$ is the set of pixels which are neighborhood of pixel at (x_0, y_0) position.

2.3.1 Variance Focus Measure (GLVA)

Variance in the specific region of an image may be used for the simplest focus measure (Subbarao and Nikzad 1993). Variance is calculated for NxN size of image area as:

$$F_{Var} = \frac{1}{N^2} \sum_{x,y \in \Omega} (I(x,y) - \bar{I})^2 \tag{2.4}$$

where I is the average of the pixel value in a chosen area and it is calculated as:

$$\bar{I} = \sum_{x,y \in \Omega} \frac{I(x,y)}{N} \tag{2.5}$$

The variance of the gray values in sharp image region is higher than that in a blur image. (Helmli and Scherer 2001).

2.3.2 Grey Level Local Variance (GLLV)

Grey Level Local Variance was proposed for autofocus of diatoms in brightfield microscopy (Pacheco et al. 2000). It is calculated as following:

$$F_{GLLV} = \sum_{(i,j)\in\Omega} (I(i,j) - \bar{I})^2 \tag{2.6}$$

where the variance of graylevels within a neighborhood of size wx+ wy centered at (i,j).

2.3.3 Normalized Grey Level Variance (GLVN)

GLVN is calculated by normalizing the value of F_{GLLV} in Equations (2.6), (Pertuz et al. 2012).

2.3.4 Modified Grey Level Variance (GLVM)

Modified gray level variance is computed as:

$$F_{GLVM} = \sum_{(i,j)\in(x,y)} (I(i,j) - \mu)^2 \tag{2.7}$$

where is obtained through a linear convolution filter, (Pertuz et al. 2012).

2.3.5 Mean Method Focus Measure (HELM)

The ratio of the center value in the neighborhood to mean value can also be used as a focus measure, (Helmli and Scherer 2001). If focus measure is one, it shows that the value of pixels have same value in this field. It means that there is no texture in the image. If there is enough pattern in the scene, image field in fully focused position will get high value. Calculated values gather around a local window like all other focus measure operator.

$$F_{Mean} = \frac{I(x,y)}{\overline{I(x,y)}} \tag{2.8}$$

2.3.6 Curvature Focus Measure (CURV)

If we assume that image pixel value is a surface in 3D space, it can be said that there are too many curvatures in a surface area where is correspond to fully focus object. Helmli and Scherer (2001) proposed to compute focus level by making surface similar to second degree polynomials. First, this method is based on the assumption that surface will fit $S(x,y)=ax+by+cx_2+dy_2$ equation. Coefficients of this equation are found using at least squares methods. Then, absoulute value of coefficients are added for the focus measure calculation.

$$F_{CURV} = |a| + |b| + |c| + |d| \tag{2.9}$$

2.3.7 Energy Gradient (GRAE)

The square of the square sum of gradient in the both directions of images are added by taking in consideration of that focus measure. (Subbarao and Nikzad 1993).

$$F_{EG} = \sum_{x,y\in\Omega} ((\frac{\partial I(x,y)}{\partial x})^2 + (\frac{\partial I(x,y)}{\partial y})^2)^2 \tag{2.10}$$

2.3.8 Tresholded Gradient (GRAT)

In this FM, first derivative is calculated as:

$$F_{Grat} = \sum_{M}\sum_{N} |I(i,j+1) - I(i,j)| \tag{2.11}$$

$$|I(i,j+1) - I(i,j)| \geq T \tag{2.12}$$

where T is the gradient threshold and I(i,j) is the grey level intensity of pixel (i,j), (Santos et al. 1997).

2.3.9 Squared Gradient (GRAS)

This FM operator is computed with squaring the difference, this is based on the assumption that the larger gradients have more influence on the final result, (Eskicioglu and Fisher 1995):

$$F_{Gras} = \sum_{M}\sum_{N} |I(i,j+1) - I(i,j)|^2 \tag{2.13}$$

$$|\mathrm{I(i,j+1) - I(i,j)}| \geq T \tag{2.14}$$

2.3.10 Tenengrad (TENG)

Tenengrad is also a focus measure operator. This is calculated by applying a high pass filter which is like a Gradient Energy to an image Tenenbaum (1971). The sum of squared components of horizontal and vertical Sobel masks is calculated in this focus measure. The result of this computation is like the Laplace focus measure summation in a local window for enhancement of the robustness.

$$\mathrm{F_{Teng}} = \sum_{\mathrm{x,y}\in\Omega} \mathrm{I_x(x,y)^2 + I_y(x,y)^2} \tag{2.15}$$

2.3.11 Tenengrad Variance (TENV)

Tenengrad Variance uses the variance of the image gradient as a FM, (Pacheco 2000).

$$F_{TENV} = \sum_{i,j\in\Omega(x,y)} (G(i,j) - \bar{G})^2 \tag{2.16}$$

where $\bar{G}$ is the mean value, G is the gradient magnitude:

$$G = \sqrt{G_x^2 + G_y^2} \tag{2.17}$$

2.3.12 Vollath's Correlation (VOLA)

Autocorrelation was proposed as a focus measure (Santos et al. 1997).

$$F_{VOLA} = \sum_{(i,j) \in \Omega(x,y)} (I(i,j) \cdot I(i+1,j) - \sum_{(i,j) \in \Omega(x,y)} I(i,j) \cdot I(i+2,j) \tag{2.18}$$

2.3.13 Vollath's Standard Deviation (VOLS)

Autocorrelation was proposed as a focus measure (Santos et al. 1997).

$$F_{VOLS} = \sum_{i=1}^{M-1} \sum_{j=1}^{N} I(i,j) \cdot I(i+1,j) - MN\bar{I}^2 \tag{2.19}$$

2.3.14 Laplacian

Taking second derivative of images is the other way of making high pass filter. Laplace operator for two dimensional images is used widely (Aydin 2011).

$$F_L = \sum_{x,y \in \Omega} \frac{\partial^2 I(x,y)}{\partial x^2} + \frac{\partial^2 I(x,y)}{\partial y^2} \tag{2.20}$$

where I(x,y) is the image intensity at the (x,y) point.

2.3.15 The Energy Laplacian

The square of the second order derivative of image pixels are added in this focus measure, (Aydin 2011).

$$F_{EL} = \sum_{x,y\in\Omega} (\frac{\partial^2 I(x,y)}{\partial x^2} + \frac{\partial^2 I(x,y)}{\partial y^2})^2 \tag{2.21}$$

2.3.16 Sum Modified Laplacian (LAPM)

The second derivatives in the vertical and horizontal directions may have opposite signs and components may cancel each other in classic Laplacian. Therefore, Nayar and Nakagawa (1994) proposed Sum Modified Laplacian. In this operator, the sum of absolute values of square of the partial second derivatives is taken instead of taking the sum of square of partial second derivatives.

$$\mathrm{F_{SML}} = \sum_{\mathrm{x,y}\in\Omega} \nabla^2\mathrm{I(x,y)}\,, \text{and } \nabla^2\mathrm{I(x,y)} > \mathrm{T} \tag{2.22}$$

$$\nabla^2 I(x,y) = \left|\frac{\partial^2 I(x,y)}{\partial x^2}\right| + \left|\frac{\partial^2 I(x,y)}{\partial y^2}\right| \tag{2.23}$$

2.3.17 Variance of Laplacian(LAPV)

Variance of the image Laplacian was proposed as a focus measure (Pacheco et al. 2000).

$$F_{LAPV} = \sum_{(i,j)\in\Omega(x,y)} (\Delta I(i,j) - \overline{\Delta I})^2 \tag{2.24}$$

where $\overline{\Delta I}$ is the mean value of the image Laplacian.

2.3.18 Diagonal Laplacian (LAPD)

Diagonal Laplacian is computed as (Thelen et al. 2009):

$$F_{LAPD} = |I * L_x| + |I * L_y| + |I * L_{x_1}| + |I * L_{x_2}| \tag{2.25}$$

where L values are convolution masks.

2.3.19 3D Laplacian

Ahmed and Choi (2007) proposed a focus measure for 3D windows instead of 2D windows. The three axes of the 3D windows are rows, columns and image frames.

2.3.20 Laplacian in 3D Window (LAP3)

3D neighborhood Laplacian was proposed as a focus measure (An et al. 2008).

$$F_{LAPV} = \sum_{f=k-1}^{k+1} \sum_{(i,j)\in\Omega(x,y)} |\Delta_M I_f(i,j)| \tag{2.26}$$

where $\Delta_M I_f$ is the modified Laplacian of f-th image.

2.3.21 Histogram Entropy (HISE)

The entropy of the image is also used for the focus mesurements (Pertuz et al. 2012).

$$\mathrm{F_{HISE}} = -\sum_{\mathrm{k=}}^{\mathrm{L}} \mathrm{P_k log(P_k)} \tag{2.27}$$

where P_k is the relative frequency k-th gray level.

2.3.22 Histogram Range (HISR)

The histogram range was proposed as a focus measure (Firestone et al. 1991) :

$$F_{HISR} = \max(k|H > 0) - \min(k|H > 0) \tag{2.28}$$

where H is the histogram within $\Omega(x, y)$ neighborhood.

2.3.23 Steerable Filter (SFIL)

Filtered version of the image I_f was proposed as a focus measure (Minhash et al. 2009).

$$F_{SFIL} = \sum_{(i,j)\in\Omega(x,y)} I_f(i,j) \tag{2.29}$$

I_f (i,j) is denoted as:

$$I_f(i,j) = max\{R^{\theta}\} \tag{2.30}$$

where R^{θ} is the image response to steerable filter:

$$R^{\theta_n} = \cos(\theta_n)\,(I * \Gamma_x) + \sin(\theta_n)\,(I * \Gamma_y) \tag{2.31}$$

with Γ_x and Γ_y are the Gaussian derivatives.

2.3.24 Spatial Frequency (SFRQ)

This operator was proposed for the fusion of multifocus images (Huang and Jing 2007).

$$F_{SFQR} = \sqrt{\sum_{(ij)\,\in\,\Omega(x,y)} I_x(i,j)^2 + \sum_{(i,j)\,\in\,\Omega(x,y)} I_y(i,j)^2} \tag{2.32}$$

where I_x and I_y are the first derivatives of an image both X and Y direction.

2.3.25 Image Moment

A new focus measure which do not use high pass filter was developed by Zhang et al., (2000), Xiong and Shafer (1997). This focus measure operator uses the theoretical results about image moments of Flusser and Suk (1998). Flusser and Suk proved that second degree moments are sensitive to bluriness. By using this finding, Zhang et al. (2000) developed a focus measure operator through using second and fourth degree moments and he proved that the operator is monotone. The disadvantage of moment based focus measure is to be sensitive to image borders. Therefore, this operator produces effective results for only foreground objects.

2.3.26 Chebyshev Moments Based Focus Measure Operator (CHEB)

Chebyshev Moments Based Focus Measure was proposed as the ratio between the energy of the high pass band and the energy of low pass band (Yap and Raveendran 2004).

$$F_{Cheb} = \frac{\left\| H(\tilde{I}; p) \right\|}{\left\| L(\tilde{I}; p) \right\|} \tag{2.33}$$

where Ĩ is the normalized image, which is computed as:

$$\tilde{\mathrm{I}} = \frac{\mathrm{I}}{\sqrt{\sum_{(\mathrm{i,j})} [\mathrm{I}(\mathrm{i}, \mathrm{j})]^2}} \tag{2.34}$$

2.3.27 Absolute Central Moment (ACMO)

Shirvaikar et al.(2004) proposed a focus measure operator which is based on statistical measures and the image histogram H:

$$F_{ACMO} = \sum_{k=1}^{L} |k - \mu| P_k \tag{2.35}$$

where μ is the mean intensity of histogram H, the number of gray level is L, P_k is the relative frequency of the k-th gray level.

2.3.28 Brenner's Focus Measure (BREN)

In this focus measure operator (Pertuz et al. 2012), second difference of the image gray levels of an image I is computed as:

$$F_{Bren} = \sum_{(ij)} |I(i,j) - I(i+2,j)|^2 \tag{2.36}$$

2.3.29 Image Contrast (CONT)

Image contrast was used as a focus measure to detect sharp pixel, (Nanda end Cutler 2001).

$$\mathrm{C(x,y)} = \sum_{\mathrm{i=x-1}}^{\mathrm{x+1}} \sum_{\mathrm{j=y-1}}^{\mathrm{y+1}} |\mathrm{I(x,y) - I(i,j)}| \tag{2.37}$$

where C(x,y) is the image contrast for pixel I(x,y). After this operation, focus measure operator is computed as:

$$F_{Cont} = \sum_{(i,j)\in\Omega(\mathrm{x,y})} C(i,j) \tag{2.38}$$

2.3.30 Eigenvalues Based Focus Measure Operator (EIGV)

The trace of the matrix of eigenvalues ∧ was proposed (Wee and Paramesran 2007).

$$F_{EIGV} = trace[\wedge_k] \tag{2.39}$$

2.3.31 Gausian Derivative Focus Measure Operator (GDER)

Geusebroek et al. (2000) proposed a focus measure for autofocus in microscopy based on the first order Gausian deriative:

$$F_{GDER} = \sum_{(x,y)} (I * \Gamma_x)^2 + (I * \Gamma_y)^2 \tag{2.40}$$

Γ is the Gaussian function, which is computed as:

$$\Gamma(x, y, \sigma) = \frac{1}{2\pi\sigma^2} \exp(-\frac{x^2 + y^2}{2\sigma^2}) \tag{2.41}$$

2.3.32 Susan Operator

This focus measure exploits image property maps which is extracted by using Susan operator, (Smith and Brady 1997). The focus level of pixels is determined by exponentially decaying function with respect to distance from extracted feature point. Focus measure is calculated for any x and y pixel position in an image as follows: (Mendapara et al., 2009):

$$\mathrm{F_{SUSAN}} = \mathrm{e}^{-(\mathrm{d(x,y)}/2)}\mathrm{I(x,y)} + (1 - \mathrm{e}^{-(\mathrm{d(x,y)}/2)}) \tag{2.42}$$

d(x,y) is the distance between nearest feature point and pixel which focus criterion will be calculated. d(x,y) is calculated by applying distance transformation to feature map which is acquired by Susan Operator .

2.3.33 Sum of Wavelet Coefficients (WAVS)

The statistical properties of the discrete wavelet transform (DWT) coefficients are used by Wavelet-based focusmeasure operators. Images split into four parts : W_{LL1}, W_{LH1}, W_{HL1} and W_{HH1}, (Pertuz et al. 2012)

$$F_{WAVS} = \sum_{(ij) \in \Omega_D} |W_{LH1}(i,j)| + |W_{HL1}(i,j)| + |W_{HH1}(i,j)| \tag{2.43}$$

2.3.34 Ratio of Wavelet Coefficients (WAVR)

The ratio of high frequency and low frequency coefficients which is obtained by applying the discret wavelet transform to images is used in this operator. Although the performance of this method is good in normal image, the performance will decrease if the noise level increases in images.

$h_w(f)$, high frequency coefficients and $l_w(f)$, low frequency coefficients is obtained by wavelet transform of a given image. The focus measure operator is found as following: (Kautsky et al. 2002, Huang et al. 2005):

$$\mathrm{F_{WAVR}} = \frac{\|\mathrm{h_W(f)}\|}{\|\mathrm{l_W(f)}\|} \tag{2.44}$$

2.3.35 Variance of Wavelet Coefficients (WAVV)

Images are transported through high pass and low pass filters using Daubechies D6 wavelet filter in this wavelet transform based method which was developed by Yang and Nelson (2003). The result of this computation, new images split into four parts : W_{LL1}, W_{LH1}, W_{HL1} and W_{HH1} . The focus measure operator is found using these parts as following:

$$F_{WAVV} = \sum_{(i,j) \in \Omega_D} (W_{LH1}(i,j) - \mu_{LH1})^2 + \sum_{(i,j) \in \Omega_D} (W_{HL1}(i,j) - \mu_{HL1})^2 + \sum_{(i,j) \in \Omega_D} (W_{HH1}(i,j) - \mu_{HH1})^2 \quad (2.45)$$

N is the window size, μ is the average pixel value of the image inside of the window.

2.3.36 The Discrete Cosine Transform (DCT)

In literature, there is also focus measure operator which is based on The Discrete Cosine Transform(DCT). (Charfi et al. 1991, Baina and Dublet 1995, Kristan et al. 2006). Images which are expressed with pixel values are turned spatial frequencies form by DCT. For this reason, the coefficients corresponding to these frequencies are calculated. Calculated values split into two parts, DC is the zero frequency coefficient, AC is the others. DCT turns image which is described by pixel value to spatial frequency type. DCT base operators calculate focus level with coefficients which is acquired by the result of image cosine transformation. Baina and Dublet (1995) showed that energy of DC coefficient of DCT can be used for the focus criterion. F(u, v) is acquired by DCT operation applied on image pixels. According to this, proposed focus criterion is calculated as:

$$F_{DCT_1} = \sum_{u,v \in \Omega} F(u,v)^2 \quad (2.46)$$

Lee et al. (2006) computed the impact of coefficients at the points which are close to the center of image block on calculated focus measure. (DCT operation was applied to this image block before.) Afterward, they showed that the effect of these coefficients are more than the effect of points close to edges. Therefore, proposed DCT based focus measure operator only computes coefficient which is found center for every image block. Computational cost is less than other focus measure operators, so devices which have limited energy like mobile phone use this measure, (Aydin 2011)

Another DCT based focus criterion was proposed by (Kristan et al., 2006). In this method, the amount of focus level in image is found with entropy calculation of normalized DCT coefficient. DCT coeficients which is applied by Bayes-distribution entropy function is called $\tilde{F}$(u,v), focus criterion is calculated as:

$$F_{DCT_2} = 1 - \sum_{u,v \in \Omega} \tilde{F}(u,v)^2 \tag{2.47}$$

2.3.37 DCT Energy Ratio (DCTE)

Shen and Chen (2006) showed that the ratio of the energies of AC and DC coefficients for low contrast images is better focus measure operator.

$$\mathrm{F_{DCTE}} = \frac{\mathrm{E_{AC}}}{\mathrm{E_{DC}}} \tag{2.48}$$

where EAC and EDC are energy of the AC and DC components of DCT respectedly.

2.3.38 DCT Reduced Energy Ratio (DCTR)

The reason of the appearance of noise in high frequency band, DCTR was proposed, (Lee et al. 2009).

$$\mathrm{F_{DCTR}} = \frac{\mathrm{S_{01}^2} + \mathrm{S_{10}^2} + \mathrm{S_{20}^2} + \mathrm{S_{11}^2} + \mathrm{S_{02}^2}}{\mathrm{S_{00}^2}} \tag{2.49}$$

where S is DCT coefficient.

2.3.39 Modified DCT (DCTM)

This focus measure operator (**Lee et al. 2008**) is obtained by using linear convolution with mask (M). It is calculated as:

$$\mathrm{F_{DCTM}} = \sum_{\mathrm{i,j}\in\Omega(\mathrm{x,y})} (\mathrm{I} * \mathrm{M}) \tag{2.50}$$

2.3.40 Energy of S Transform

The Stockwell Transform (S-transform) (Stockwell et al. 1996) is used image processing and signal processing widely because of its advantages over frequency analysis tools like wavelet transform and fourier transform. Mahmood and Choi (2010) used S transform as a focus measure operator. Focus measure is found with the asumption that performed S transform of image is I_{SD}:

$$F_{SD} = \sum_{u,v\in\Omega} I_{SD}(u,v)^2 \tag{2.51}$$

2.3.41 Bipolar Image Filter

Malik and Choi (2008) exploited bipolar incoherent image processing (Poon 1985, Indebetouw and Poon 1986) to develop focus measure which is insensitive to noise. In this focus measure images pass through the bipolar (h) filter to get I_c images.

$$I_c = I * h(\sigma_1, \sigma_2) \tag{2.52}$$

where σ_1 and σ_2 are bipolar filter, * shows the convolution operations. Focus measure operator is found by using acquiered images as:

$$F_{PLR} = \sum_{x,y\in\Omega} I_c\,(x,y) \tag{2.53}$$

Apart from these, there are focus measure operators which exploit different functions like image entropy (Bove 1993), power-spectra analysis (Jutamulia et al. 1994), gabor filter (Xiong and Shafer 1994), orientation code matching (Li et al. 2007), shapelet decomposition (Meneses et al. 2008), principal component analysis on DCT based (Mahmood et al. 2008) and wavelet based (Mahmood et al. 2009). In literature, there are several studies on performance comparison for different situations of different focus measure operators. (Groen et al. 1985, Subbarao and Tyan 1998, Huang and Jing, 2007; Tian et al. 2007, Aslantas and Kurban 2009).

2.4 IMAGE QUALITY METRICS

Assesment of the image quality has a great impact on image processing because it is difficult task for computers to reveal the difference between two images without human interfere. For this reason, many metrics are proposed to show image quality. These metrics are based on different techniques such as pixel difference, human visual system (Al-Najjar and Chen 2012).

In order to determine which result of focus measure operator is better, five quality metrics are used in this study.

i. Structural Similarity Index (SSIM):

Wang et al. (2004) proposed Structural Similarity Index which is based on the comparision of luminance, contrast and structure. In this index, image degradations are considered as a perceived changes in structural information. However, the other approches which is based on the error sensitivity used perceived errors to quantify image degredation.

$$\mathrm{SSIM}(x,y) = \frac{(2\mu_x\mu_y + c_1)(2\sigma_{xy} + c_2)}{(\mu_x{}^2 + \mu_y{}^2 + c_1)(\sigma_x{}^2 + \sigma_y{}^2 + c_2)} \tag{2.54}$$

where μ is the mean value of an image, σ^2 is the variance of an image, c is the constant.

ii. Peak Signal-to-Noise Ratio (PSNR)

PSNR is the ratio between the maximum possible value of a signal and the corrupting noise which causes distortion of the image. The maximum possible value of image pixel is 255 when pixels are 8 bits (uint8 image). Therefore, PSNR is computed as:

$$\text{PSNR} = 10 \log \frac{s^2}{MSE} \tag{2.55}$$

where s is the maximum possible value and MSE is the mean square error.

iii. Normalized Cross Correlation

Capturing images with different aperture and focal settings causes different brightness on images. This situation leads comparision problem. In order to compensate this, normalized cross correlation is used as:

$$\text{NCC} = \frac{\sum_{m=1}^{M} \sum_{n=1}^{N} I(m,n).I'(m,n)}{\sum_{m=1}^{M} \sum_{n=1}^{N} I^2(m,n)} \tag{2.56}$$

where I is the reference image and I' is the other image.

iv. Mean Square Error

Mean square error (MSE) has been widely used for the computation of image quality. It is calculated by averaging the square intensity of the reference image and reconstructed image pixels. This metric is based on the pixel difference.

$$\text{MSE} = \frac{1}{MN} \sum_{m=1}^{M} \sum_{n=1}^{N} e(m,n)^2 \tag{2.57}$$

where e(m,n) is pixel value which is acquired by taking difference between output and input images. M and N are size of an image.

v. Normalized Absolute Error

NAE is computed by normalizing of absolute difference between the reference image and reconstructed image.

$$\text{NAE} = \frac{\sum_m^M \sum_n^N |e(m,n)|}{\sum_m^M \sum_n^N |I(m,n)|} \tag{2.58}$$

where e(m,n) is pixel value which is acquired by taking difference between output and input images. M and N are size of an image.

3. EXPERIMENTS

3.1 TEST ON REAL DATA AND SYNTHETIC DATA

In this experiment, tests are performed on real data and synthetic data. Two kind of image sequences which were captured using a real apeture camera have been used as real data. First one is the real focus sequence of 27 images of 510 x 600 pixels (Mozart Image) and the other one is the real focus sequence of 14 images of 614 x 819 pixels (Deer Image). Images which belong to one sequence was acquired with different focus settings from same scene. Synthetic image was generated with Iris filter from real all focus image. There are 32 images of 383 x 434 pixels in this focus sequence (Venus Image). Real all focused images (referenced images) were captured with the smallest aperture size for the three scenes.

3.2 METHOD

In this part, operations which are applied to get all in focus image are explained. First of all, Focus Measure is computed for every image in the sequence. Thirty five different focus measure operators in the litarature were used for calculation in this experiment. FM operators require neighborhood operation to compute the focus value of every pixel. Therefore, window size is chosen 3 x 3.

$$v_i = FM(I_i) \tag{3.1}$$

where I is image, i=1…N, N is the number of images in a sequence
Then, maximum focus measure is chosen from v which is hold focused measure of all images. D is the depth of the scene. Depth of the scene is exploited to find pixel position in the focused image.

$$[FMsD] = \max(v) \tag{3.2}$$

After finding maximum focus measure positions, pixels in those positions are taken to acquire all in focus image.

$$I = I_s(D) \tag{3.3}$$

where I_s is the image stack.

At the end of these operations, efficiency of the focus measure operators are mesuared with five image quality metrics. These metrics are Structural Similarity Index (SSIM), Peak Signal-to-Noise Ratio (PSNR), Normalized Cross Correlation, Mean Square Error, Normalized Absolute Error.

3.3 COMPARISION OF FOCUS MEASURE OPERATORS

Five quality metrics were used in order to compare reference image and All In Focused images which were acquired with different focus measure operators. Two tables were created for every image sequence. One table is the combination of best five results according to quality metric values. Second table is the combination of poorest five image according to quality metric values.

3.3.1 Deer Images

Table 3.1 shows the best results according to quality metrics for Deer Sequence.

Table 3.1: Best results according to quality metrics for Deer Sequence

Focus Measure Operator	SSIM	Focus Measure Operator	PSNR	Focus Measure Operator	Normalized Cross Correlation	Focus Measure Operator	Mean Square Error	Focus Measure Operator	Normal Absolute Error
VOLS	0,57	VOLS	13,93	DCTE	5,55E-10	VOLS	2631,25	VOLS	0,35642
WAVR	0,517	ACMO	12,51	WAVR	5,56E-10	ACMO	3645,85	ACMO	0,43669
HELM	0,516	HISE	12,4	DCTR	5,57E-10	HISE	3744,73	HISE	0,44164
DCTE	0,515	GDER	12,4	WAVV	5,65E-10	GDER	3744,89	GDER	0,44165
DCTR	0,513	BREN	12,27	GLVM	5,66E-10	BREN	3855,1	HELM	0,44867

According to Table 3.1, image which was acquired using VOLS operator get good result for every metrics except Normalized Cross Correlation. Figure 3.1 shows Image Comparision, right side image is Reference Image and left side image is VOLS result.

VOLS Result is not sharp enough and edges are not clear compared to Reference Image. In Figure 3.2, it can be seen some drawings on the wall and it is more sharp than VOLS result but some area are not have enough information to complete shape. WAVR result in Figure 3.3, which is second best for SSIM and Normalized Cross Correlation Metrics have more information than DCTE in Figure 3.2.

Figure 3.1: Image Comparision (Left side image is obtained with VOLS operator, Right side image is Reference Image)

Figure 3.2: Image which is acquired with DCTE

Figure 3.3: Image which is acquired with WAVR

Table 3.2 and Tablo 3.3 contain ACMO operators, some metrics evaluated it as a good result like PSNR, MSE, NAE. Even if forefront object is clear in the ACMO image, some regions are blurry. CURV is blurry and it is interpreted as a bad result by all metrics.

Table 3.2: Poor result according to quality metrics for Deer Sequence

Focus Measure Operators	SSIM	Focus Measure Operator	PSNR	Focus Measure Operator	Normalized Cross Correlation	Focus Measure Operator	Mean Square Error	Focus Measure Operator	Normal Absolute Error
CHEB	0,384	CURV	10,87	CURV	6,31E-10	CURV	5317,99	CURV	0,55333
GDER	0,412	VOLA	11,44	ACMO	6,16E-10	VOLA	4670,15	VOLA	0,50917
HISE	0,412	DCTM	11,97	VOLA	6,09E-10	DCTM	4131,18	DCTM	0,47088
VOLA	0,413	GLLV	12,02	SFIL	6,05E-10	GLLV	4080,56	GLLV	0,46346
ACMO	0,42	DCTE	12,04	CHEB	6,01E-10	DCTE	4064,01	TENV	0,46262

i. SSIM:

If SSIM quality metrics is high, the result image is more closer to reference image. Following five images got higher SSIM values and they are sharp. CHEB, GDER HISE, VOLA, ACMO got low and they are not sharp.

Figure 3.4: The maximum SSIM value order for Deer Sequence

Figure 3.5: The minimum SSIM value order for Deer Sequence

ii. PSNR:

If PSNR is high, the better results will be obtained. However, ACMO, GDER and HISE got high value, they are blurry and GLLV and DCTE got minimum result, the image quality is high.

Figure 3.6: The maximum PSNR value order for Deer Sequence

Figure 3.7: The minimum PSNR value order for Deer Sequence

iii. Normalized cross correlation (NCC):

If this metric is low, the result is better. Minimum NCC values were acquired for DCTE, WAVR, DCTR, WAVV, GLVM and these operators have sharp results for all in focus image. CURV, ACMO, VOLA, SFIL and CHEB have maximum NCC and the result images are blurry as in:

Figure 3.8: The maximum Normalized Cross Correlation value order for Deer Sequence

Figure 3.9: The minimum Normalized Cross Correlation value order for Deer Sequence

iv. Mean Square Error:

If this metric is high, image quality will be poor. In this metric, CURV, VOLA DCTM images which have poor quality got maximum metric results. GLLV and DCTE also got maximum mean square error but image quality is high.

Figure 3.10: The maximum Mean Square value order for Deer Sequence

Figure 3.11: The minimum Mean Square Error value order for Deer Sequence

v. Normalized Absolute Error:

This metric is based on error, therefore minimum error between reference image and all in focused image gives good result. VOLS, HELM have minimum NAE and images are sharp, but other images which got minimum result are blurry (ACMO, HISE, GDER). GLLV and TENV are also sharp but they have maximum result.

Figure 3.12: The maximum Normalized Absolute Error value order for Deer Sequence

Figure 3.13: The minimum Normalized Absolute Error value order for Deer Sequence

vi. Time:

Some computation of focus measure operators took more time than others. The most time consuming five operators are CONT, ACMO, DCTE, DCTR and CHEB. The minimum time consuming five operators are BREN, GLVM, GRAE,GRAT and LAPM. In deer images, Bren operators took minimum time 11,91 seconds in Table 3.3. Even if Bren operators took a little time, better result was obtained according to PSNR and Mean Square Error Metric. GLVM is top five in Normalized Cross Correlation and took 12,07 seconds. ACMO and CHEB gave blurry results and took a lot of times.

Figure 3.14: The maximum elapsed time order for Deer Sequence

Figure 3.15: The minimum elapsed time order for Deer Sequence

Table 3.3: Focus measure and Time for Deer Sequence

FM	Time	FM	Time	FM	Time	FM	Time
BREN	11,91	SFRQ	12,24	GLLV	12,58	WAVR	14,40573
GLVM	12,08	LAPE	12,28	HISR	12,6	HISE	14,71386
GRAE	12,11	GLVN	12,31	DCTM	12,64	CHEB	452,582
GRAT	12,13	LAPV	12,35	HELM	12,66	DCTR	456,5858
LAPM	12,14	TENG	12,38	GRA3	12,77	DCTE	463,4633
GRAS	12,17	GLVA	12,45	GDER	12,79	ACMO	515,1691
VOLS	12,2	LAPD	12,45	SFIL	12,87	CONT	1157,557
VOLA	12,23	LAP3	12,48	WAVS	13,42		
CURV	12,23	TENV	12,56	WAVV	13,83		

3.3.2 Mozart Images

VOLS operators got high results from all metrics except Normalized Cross Correlation like Deer sequence. ACMO has bad quality but it is in this table. Error based operators interpreted it as good.

Table 3.4: Best results according to quality metrics for Mozart Sequence

Focus Measure Operators	SSIM	Focus Measure Operator	PSNR	Focus Measure Operator	Normalized Cross Correlation	Focus Measure Operator	Mean Square Error	Focus Measure Operator	Normalized Absolute Error
VOLS	0,342	VOLS	16,66	WAVR	5,09E-10	VOLS	1402,01553	VOLS	0,20888
WAVR	0,322	ACMO	15,28	HELM	5,09E-10	ACMO	1925,68244	ACMO	0,24824
DCTR	0,322	GDER	15,28	WAVV	5,10E-10	GDER	1925,68244	GDER	0,24824
HELM	0,321	HISE	15,28	GLVM	5,10E-10	HISE	1925,6824	HISE	0,24824
DCTE	0,32	CHEB	14,79	WAVS	5,10E-10	CHEB	2159,0092	CHEB	0,26052

WAVV, WAVS, CHEB, ACMO is found both two table. In Table 3.5, CURV is evaluated as a bad result for all metrics. The image is too bright and some regions are not clear.

Figure 3.16: Image which is acquired with CURV

Table 3.5: Poor result according to quality metrics for Mozart Sequence

Focus Measure Operators	SSIM	Focus Measure Operator	PSNR	Focus Measure Operator	Normalized Cross Correlation	Focus Measure Operator	Mean Square Error	Focus Measure Operator	Normalized Absolute Error
ACMO	0,244	CURV	12,87	ACMO	5,7948E-10	CURV	3356,79939	CURV	0,34471
GDER	0,244	VOLA	13,52	GDER	5,7948E-10	VOLA	2891,16846	VOLA	0,31756
HISE	0,244	WAVV	14,2	HISE	5,7948E-10	WAVV	2471,38989	WAVV	0,28689
CURV	0,253	WAVS	14,22	VOLS	5,576E-10	WAVS	2462,4435	WAVS	0,28647
CHEB	0,255	LAPD	14,23	CHEB	5,5355E-10	LAPD	2457,6151	HISR	0,28644

i. SSIM:

Correct results are obtained for images which was acquired with WAVR, DCTR, HELM, DCTE. However, VOLS image does not have sharp edges.

Figure 3.17: The maximum SSIM value order for Mozart Sequence

Figure 3.18: The minimum SSIM value order for Mozart Sequence

ii. PSNR:

Although HISE, GDER, ACMO and CHEB images have poor quality, PSNR values are large. WAVV, WAVS and LAPD have better quality, even if they got low result.

Figure 3.19: The maximum PSNR value order for Mozart Sequence

Figure 3.20: The minimum PSNR value order for Mozart Sequence

iii. Normalized Cross Correlation:

The operation of WAVR, HELM, WAVV, GLVM, WAVS took between 8 and 10 seconds. The images are sharp and they evaluated correct by NCC.

Figure 3.21: The maximum Normalized Cross Correlation value order for Mozart Sequence

Figure 3.22: The minimum Normalized Cross Correlation order for Mozart Sequence

iv. Mean Square Error:

Mean square errors of WAVV, WAVS and LAPD are high, it means that these images are not similar reference image, but they are sharp.

Figure 3.23: The maximum Mean Square Error value order for Mozart Sequence

Figure 3.24: The minimum Mean Square Error value order for Mozart Sequence

v. Normalized Absolute Error:

Inaccurate results were obtained for WAVV, WAVS, HISR which are sharp image. ACMO, GDER, HISE, CHEB were also interpreted incorrect.

Figure 3.25: The maximum Normalized Absolute Error value order for Mozart Sequence

Figure 3.26: The minimum Normalized Absolute Error value order for Mozart Sequence

vi. Time:

The most time consuming five operators are CONT, ACMO, DCTE, DCTR and CHEB. The minimum time consuming five operators are GRAS, GLVM, DCTM and GRAT. CONT computation took 1294 seconds which is maximum elapsed time in Table 3.6 and the quality of the image is tolerable. DCTE and DCTR which have better quality according to SSIM also took a long time. GRAS, GLVM, LAPE and GRAT took less time and the result image is tolerable but DCTM is blurry.

Figure 3.27: The maximum elapsed time order for Mozart Sequence

Figure 3.28: The minimum elapsed time order for Mozart Sequence

Table 3.6: Focus measure and Time for Mozart Sequence

FM	Time	FM	Time	FM	Time	FM	Time	FM	Time
GRAS	7,991	BREN	8,08119	GLVN	8,23	CURV	8,611	HISE	11,1711
GLVM	8,0208	LAPM	8,08528	GLVA	8,24	LAP3	8,693	EIGV	250,281
DCTM	8,0349	GRAE	8,11181	SFRQ	8,24	GRA3	9,039	CHEB	449,306
LAPE	8,0357	GDER	8,16687	LAPD	8,25	SFIL	9,106	DCTR	514,013
GRAT	8,055	TENG	8,18252	HISR	8,33	WAVS	9,336	DCTE	539,263
VOLA	8,0748	LAPV	8,19025	TENV	8,34	WAVV	9,858	ACMO	596,585
VOLS	8,0772	HELM	8,23222	GLLV	8,55	WAVR	10,47	CONT	1294,73

3.3.3 Venus Images

WAVR result is chosen closer image to reference image by all metrics. HELM is also in best five measure in Table 3.7.

Table 3.7: Best result according to quality metrics for Venus Sequence

Focus Measure Operators	SSIM	Focus Measure Operator	PSNR	Focus Measure Operator	Normalized Cross Correlation	Focus Measure Operator	Mean Square Error	Focus Measure Operator	Normalized Absolute Error
WAVR	0,971	HELM	29,4	CHEB	2,05E-09	HELM	74,6094801	WAVR	0,04576
HELM	0,971	TENV	29,32	VOLA	2,07E-09	TENV	75,9928108	HELM	0,04593
GLVM	0,968	GLLV	29,32	CURV	2,09E-09	GLLV	76,0740937	GLVM	0,04731
LAPD	0,968	WAVR	29,26	DCTM	2,10E-09	WAVR	77,120766	LAPE	0,04747
LAPE	0,968	DCTE	29,05	WAVR	2,11E-09	DCTE	80,9940922	LAPD	0,04776

HISE, CURV, ACMO, VOLA and GDER were evaluated as having poor quality for all quality metrics except Normalized Cross Correlation in Table 3.8. It can be seen that these images are blurry.

Table 3.8: Poor Result According to Quality Metrics for Venus Sequence

Focus Measure Operators	SSIM	Focus Measure Operators	PSNR	Focus Measure Operators	Normalized Cross Correlation	Focus Measure Operators	Mean Square Error	Focus Measure Operators	Normalized Absolute Error
HISE	0,882	CURV	21,68	VOLS	2,24E-09	CURV	441,385701	CURV	0,11205
GDER	0,882	HISE	22,69	GRA3	2,18E-09	HISE	349,867581	HISE	0,11023
ACMO	0,882	GDER	22,69	GLVN	2,18E-09	GDER	349,867581	GDER	0,11023
CURV	0,898	ACMO	22,69	HISR	2,17E-09	ACMO	349,86758	ACMO	0,11023
VOLA	0,907	VOLA	22,84	CONT	2,16E-09	VOLA	337,750581	VOLA	0,09446

i. SSIM:

Images which take maximum SSIM values, have good quality as expected and they are sharp. Images which take minimum SSIM values, have poor quality and they have bluriness. The SSIM results are correct for following images.

Figure 3.29: The maximum SSIM value order for Venus Sequence

Figure 3.30: The minimum SSIM value order for Venus Sequence

ii. PSNR:

Images which take maximum PSNR values, have high quality as expected and they are clear. Venus word on Newspaper can seen easily and it is legible in the images. Images which take minimum PSNR values, have poor quality and they have bluriness. The PSNR results are correct for following images.

Figure 3.31: The maximum PSNR value order for Venus Sequence

Figure 3.32: The minimum PSNR value order for Venus Sequence

iii. Normalized Cross Correlation:

The result images of CHEB, VOLA, CURV, DCTM have poor quality but NCC showed them high quality. Images of GLVN, HISR and CONT are sharp but NCC values are maximum.

Figure 3.33: The maximum Normalized Cross Correlation value order for Venus Sequence

Figure 3.34: The minimum Normalized Cross Correlation value order for Venus Sequence

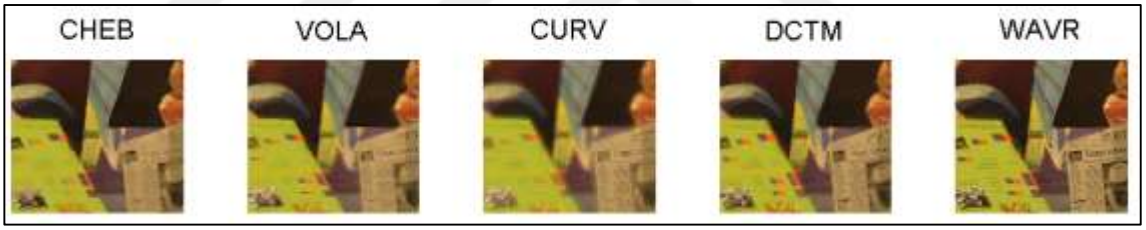

iv. Mean Square Error:

Images which take maximum MSE, have poor quality as expected and they are not clear. CURV, HISE, GDER, ACMO, VOLA have maximum MSE value and the result images are blurry. HELM, TENV, GLLV, WAVR, DCTE have minimum NAE value and the result images are sharp.

Figure 3.35: The maximum Mean Square value order for Venus Sequence

Figure 3.36: The minimum Mean Square Error value order for Venus Sequence

v. Normalized Absolute Error:

Images which take maximum NAE, have poor quality as expected and they are not clear. CURV, HISE, GDER, ACMO, VOLA have maximum NAE value and the result images are blurry. WAVR, HELM, GLVM, LAPE, LAPD have minimum NAE value and the result images are sharp.

Figure 3.37: The maximum Normalized Absolute Error value order for Venus Sequence

Figure 3.38: The minimum Normalized Absolute Error value order for Venus Sequence

vi. Time:

In Venus Sequence, the most time consuming five operators are CONT, ACMO, DCTE, CHEB and DCTR. The minimum time consuming five operators are GRAS, GLVM, GRAE, VOLA and GRAT. Even if the elapsed times for CHEB, ACMO are too much,

the results are not good. CONT, DCTE and DCTR images are sharp but elapsed times are too long in Table 3.9.

Figure 3.39: The maximum elapsed time order for Venus Sequence

Figure 3.40: The minimum elapsed time order for Venus Sequence

Table 3.9: Focus measure and time for Venus Sequence

FM	Time	FM	Time	FM	Time	FM	Time	FM	Time
GRAS	4,5468	DCTM	4,60658	GDER	4,77	HISR	5,208	CURV	6,73266
GLVM	4,5693	LAPE	4,61805	LAPD	4,78	SFIL	5,223	EIGV	162,088
GRAE	4,5742	SFRQ	4,66016	TENV	4,82	WAVS	5,512	DCTR	318,94
VOLA	4,5754	TENG	4,66255	GLLV	4,86	WAVV	5,718	CHEB	395,421
GRAT	4,5918	GLVN	4,67587	GLVA	4,9	WAVR	6,223	DCTE	452,103
VOLS	4,6031	HELM	4,69629	LAP3	5,04	BREN	6,239	ACMO	512,879
LAPM	4,6036	LAPV	4,70034	GRA3	5,2	HISE	6,506	CONT	1116,64

For real data, SSIM and Normalized Cross Correlation gave accurate result. It means that if All In Focus images which were acquired with different focus criterions are sharp and more informative, the metric may show them close to reference image. SSIM and NCC showed them correctly. The other metrics like NAE, MSE and PSNR are not sufficient to show them correctly. However, for synthetic data, SSIM, PSNR, MSE and NAE gave accurate result. In this data, Normalized Cross Correlation does not give correct result.

ACMO, CHEB, CURV, DCTM, GDER, HISE, SFIL and VOLA result is blurry for all image sequence and the elapsed times for ACMO, CHEB are too much.
DCTE and DCTR gave high quality but elapsed time is too long.

HELM, GLVR, GLVM, WAVR, WAVV mesuare operators are efficient because the results are good and elapsed times are short.

3.4 EVALUATING THE WINDOW SIZE FOR MOZART IMAGE

The larger window sizes provide to consider the more neighborhood pixels. This situation causes blurriness in the image because the number of pixels being extracted increase in the low illumination region. (Malik and Choi 2007). Therefore, it is necessary to find optimum window size. In this study, 3x3, 5x5 and 7x7 window size was eavaluated. For this reason, window size was increased to observe changes. This experiment applied Mozart Images. SSIM and Normalized Cross Correlation were exploited to evaluate results.

When the window size increased, elapsed time increased too. It can be seen all images which was acquired with different focus measures. For example, elapsed times for ACMO measurment are 596,5853 seconds in 3x3, 620,75 seconds in 5x5, 645,6489 in 7x7.

Table 3.10 and Table 3.12 show the best All In Focus Results. It can be seen that when the window size increase, the results are more better. For example, Normalized Cross Correlation of All in Focus Image which was acquired with using WAVR decrease when the window size increase. It means that the quality of the All In Focus image in 7x7 is better than All in Focus image in 3x3.

Table 3.10: Best results according to Normalized Cross Correlation

Mozart 3x3	Normalized Cross Correlation	Time	Mozart 5x5	Normalized Cross Correlation	Time	Mozart 7x7	Normalized Cross Correlation	Time
WAVR	5,0914E-10	10,5	'HELM'	5,0849E-10	8,656	'HELM'	5,0797E-10	9,801
HELM	5,092E-10	8,23	'GLVM'	5,086E-10	8,379	'GLVM'	5,0814E-10	9,312
WAVV	5,0988E-10	9,86	'WAVR'	5,0862E-10	10,74	'WAVV'	5,0829E-10	10,92
GLVM	5,0993E-10	8,02	'WAVV'	5,0882E-10	10,15	'LAPE'	5,0835E-10	9,154
WAVS	5,0997E-10	9,34	'WAVS'	5,0896E-10	9,596	'WAVR'	5,0837E-10	11,17

Table 3.11: Poor results according to Normalized Cross Correlation

Mozart 3x3	Normalized Cross Correlation	Time	Mozart 5x5	Normalized Cross Correlation	Time	Mozart 7x7	Normalized Cross Correlation	Time
ACMO	5,7948E-10	597	'ACMO'	5,7948E-10	620,8	'ACMO'	5,7948E-10	645,6
GDER	5,7948E-10	8,17	'HISE'	5,7948E-10	12,44	'HISE'	5,7948E-10	14,79
HISE	5,7948E-10	11,2	'VOLS'	5,5314E-10	8,435	'VOLS'	5,5117E-10	8,775
VOLS	5,5758E-10	8,08	'VOLA'	5,4705E-10	8,387	'DCTM'	5,4233E-10	9,196
CHEB	5,5355E-10	449	'CHEB'	5,4503E-10	512,1	'VOLA'	5,3794E-10	8,862

Table 3.11 shows the poorest five results according to Normalizes Cross Correlation. ACMO results did not change during this evaluation. However, GDER (AIF Image) with 7x7 window size is not in 7th column of the Table 3.12

Table 3.12: Best results according to SSIM

Mozart 3x3	SSIM	Time	Mozart 5x5	SSIM	Time	Mozart 7x7	SSIM	Time
VOLS	0,3421	8,08	'VOLS'	0,33188	8,435	'DCTR'	0,32485	568,2
WAVR	0,32229	10,5	'DCTR'	0,3236	563,7	'HELM'	0,32377	9,801
DCTR	0,32159	514	'HELM'	0,3234	8,656	'DCTE'	0,32288	577,2
HELM	0,32103	8,23	'WAVR'	0,32263	10,74	'EIGV'	0,32273	409,7
DCTE	0,3196	539	'DCTE'	0,32147	567,9	'WAVR'	0,32242	11,17

In Table 3.13, ACMO result did not change according to SSIM. It is the same as Normalized Cross Correlation. CHEB results is better according to rising window size.

Table 3.13: Poor results according to SSIM

Mozart 3x3	SSIM	Time	Mozart 5x5	SSIM	Time	Mozart 7x7	SSIM	Time
ACMO	0,24407	597	'ACMO'	0,24407	620,8	'ACMO'	0,24407	645,6
GDER	0,24407	8,17	'HISE'	0,24407	12,44	'HISE'	0,24407	14,79
HISE	0,24407	11,2	'CURV'	0,24862	9,493	'CURV'	0,25234	9,637
CURV	0,25287	8,61	'CHEB'	0,26322	512,1	'CHEB'	0,27399	528,9
CHEB	0,25471	449	'VOLA'	0,27501	8,387	'VOLA'	0,27992	8,862

Figure 3.41: Images acquired with CHEB using different window sizes (Left is W=3, Middle W=5, Right W=7)

Figure 3.41 shows the quality improvements respect to increasing window size. However, AIF Image which is acquired with CHEB in 7x7 window size is stil blurry. 7x7 window size for CHEB may not be optimum window size.

4. CONCLUSION

In this thesis, All In Focus Images Methods were searched, different focus measure operators and their results on All In Focus Images were examined. Tests were performed on two kind of datas which are real data and synthetic data. Real focus sequence of 27 images of 510 x 600 pixels (Mozart Sequence) and 14 images of 614 x 819 pixels (Deer Sequence) were used as a real data. Each image of a sequence was captured with different focus settings from same scene. . Synthetic data was generated with Iris filter from real all focus image. There are 32 images of 383 x 434 pixels in this focus sequence (Venus Image). Real all focused images (referenced images) were captured with the smallest aperture size both three scenes.

Three steps were followed in this study. First two steps are related to acquiring AIF Image. Firstly, Focus Measure was computed for every image in the sequence. Thirty five different focus measure operators in the litarature was used for this operation. Secondly, maximum focus measure was chosen because maximum focus measure indicates focused area. Finally, images were combined together to get a new image where all the objects are in focus.

After these computation, five quality metrics were used to compare reference image and acquiered all in focus image. These metrics are Structural Similarity Index (SSIM), Peak Signal-to-Noise Ratio (PSNR), Normalized Cross Correlation, Mean Square Error, Normalized Absolute Error.

For real data, SSIM and Normalized Cross Correlation gave accurate result. It means that if all in focus images which were acquired with different focus criterions are sharp and more informative, the metric may show them close to reference image. SSIM and NCC showed them correctly. The other metrics like NAE, MSE and PSNR were not sufficient to show them correctly. However, for synthetic data, SSIM, PSNR, MSE and NAE gave accurate result. In this data, Normalized Cross Correlation did not give correct result.

ACMO, CHEB, CURV, DCTM, GDER, HISE, SFIL and VOLA result is blurry for all image sequence and the elapsed times for ACMO, CHEB are too much. DCTE and DCTR gave high quality but elapsed time is too long. HELM, GLVR, GLVM, WAVR, WAVV mesuare operators are efficient because the results are good and elapsed times are short.

In addition to that, window size which is used for the operation of focus measure criterions is searched. Window size is increased gradually. (3x3,5x5,7x7) When the window size increased, elapsed time increased too. The image quality is increase except some operators like ACMO.

REFERENCE

Books

Born, M. and Wolf, E., 1965. Principles of Optics: Electromagnetic Theory of Propagation, Interference and Diffraction of Light. 3. Edition. NY :Pergamon Press.

Periodicals

Aguet, F., De Ville, D. V. and Unser, M., 2008. Model-based 2.5-D deconvolution for extended depth of field in brightfield microscopy. *IEEE Trans. Image Process*. **17**(7), pp. 1144–1153.

Ahmad, M. and Choi, T.S., 2007. Application of three dimensional shape from image focus in lcd/tft displays manufacturing. *IEEE Trans. Consumer Electronics*. **53**, pp. 1–4.

Al-Najjar, Y. and Chen, S., 2012.Comparison of Image Quality Assessment: PSNR, HVS, SSIM, UIQI. *International Journal of Scientific & Engineering Research*. **3(**8).

An, Y., Kang, G., Kim, I., J., Chung, H. S. and Park, J., 2008. Shape from focus through Laplacian using 3D window. *In International Conference on Future Generation Communication and Networking*. **2**, pp. 46–50.

Antunes, M., Trachtenberg, M., Thomas, G. and Shoa, T., 2005. All-in-focus imaging using a series of images on different focal planes. *In Proc. Image Anal. Recognit. Conf*. pp. 174–181.

Aslantas, V., and Pham, D.T., 2007. Depth from automatic defocusing. *Optics Express*.**15**, pp. 1011-1023.

Aslantas, V. and Kurban, R., 2009. A comparison of criterion functions for fusion of multi-focus noisy images. *Optics Communications*. **282**(16), pp. 3231 – 3242.

Aslantas, V., Toprak, A.N., Kurban Bendeş E., 2013. Çoklu-odaklı görüntülerin genetik algoritma kullanılarak birleştirilmesi. *Sigma*. **5**, pp. 25-37.

Avcibas,I., Sayood, K. and Sankur, B., 2002. Statistical Evaluation of Quality Measures in Image Quality Compression. *Journal of Electronic Imaging*. **11**(2), pp.206–223

Baina, J. and Dublet, J., 1995. Automatic focus and iris control for video cameras. pp. 232 –235.

Bove, J. M., 1993. Entropy-based depth from focus. *J. Opt. Soc. Am. A*. **10**(4), pp. 561–566.

Charfi, M., Nyeck, A. and Tosser, A., 1991. Focusing criterion. *Electronics Letters*. **27**(14), pp. 1233 –1235.

Darrell, T. and Wohn, K., 1988. Pyramid based depth from focus. In Proceedings of IEEE Conference on Computer Vision and Pattern Recognition, pp.504-509.

Eskicioglu, A.M. and Fisher, P.S., 1995. Image quality measures and their performance. *IEEE Transactions on Communications*. **43**, pp. 2959–2965.

Firestone, L., Cook, K., Culp, K., Talsania, N. and Preston, K., 1991.Comparison of auto focus methods for automated microscopy. *Cytometry*. **12**, pp.195–206.

Flusser, J. and Suk, T., 1998. Degraded image analysis: an invariant approach. *Pattern Analysis and Machine Intelligence, IEEE Transactions.* **20**(6), pp. 590–603.

Forster, B., De Ville, D. V., Berent, J., Sage, D. and Unser, M., 2004. Complex wavelets for extended depth-of-field: A new method for the fusion of multichannel microscopy images. *Microsc. Res. Tech*. **65**(1–2), pp. 33–42.

Geusebroek, J., Cornelissen, F., Smeilders, A. and Geerts, H., 2000. Robust autofocusing in microscopy. *Cytometry*. **39**, pp. 1–9.

Groen, F. C., Young, I. T., and Ligthart, G., 1985. A comparison of different focus functions for use in autofocus algorithms. *Cytometry*. **6**(2), pp. 81–91.

Helmli, F. and Scherer, S., 2001. Adaptive shape from focus with an error estimation light microscopy. Image and Signal Processing and Analysis. pp.188–193.

Huang, J.T., Shen, C.H., Phoong, S.M. and Chen, H., 2005. Robust measure of image focus in the wavelet domain. *Proceedings of the International Symposium on Intelligent Signal Processing and Communication Systems.* pp. 157 – 160.

Huang, W. and Jing, Z., 2007. Evaluation of focus measures in multi-focus image fusion. *Pattern Recognition Letters*. **28**, pp. 493–500.

Indebetouw, G. and Poon, T. C., 1986. Parallel synthesis of bipolar point spread functions in a scanning heterodyne optical system. *Optica Acta: International Journal of Optics.* **33** (7), pp. 827–834.

Jutamulia, S., Asakura, T., Bahuguna, R. D., and DeGuzman, P. C., 1994. Autofocusing based on power-spectra analysis. *Appl. Opt*. **33**(26), pp. 6210–6212.

Kautsky, J., Flusser, J., Zitová, B., and Simberová, S., 2002. A new wavelet-based measure of image focus. *Pattern Recognition Letters.***23**(14), pp. 1785 – 1794.

Kodama, K., Aizawa, K. and Hatori, M., 1996. Iterative Reconstruction of an All-Focused Image by Using Multiple Differently Focused Images. *IEEE Proceedings of 1996 International Conference on Image Processing*. **3**, pp.551-554.

Kodama, K., Mo, H. and Kubota, A., 2007. Simple and fast all-in-focus image reconstruction based on three-dimensional/two-dimensional transform and filtering. *In Proc. IEEE Int. Conf. Acoust. Speech Signal Process*.**1**, pp. 769–772.

Kristan, M., Pers, J., Perse, M. and Kovacic, S., 2006. A bayes-spectralentropy-based measure of camera focus using a discrete cosine transform. *Pattern Recognition Letters*. **27**(13), pp. 1431 – 1439.

Lee, S., Park, S., Kim, C., Kumar, Y. and Kim, S., 2006. Low-power auto focus algorithm using modified dct for the mobile phones. pp. 67 – 68.

Lee, S.Y., Kumar, Y., Cho, J. M., Lee, S.W. and Kim, S.W., 2008. Enhanced auto focus algorithm using robust focus measure and fuzzy reasoning. *IEEE Transactions on Circuits and Systems for Video Technology*. **18**, pp. 1237–1246.

Lee, S.Y., Yoo, J.T, Kumar, Y. and Kim, S.W., 2009. Reduced energy-ratio measure for robust auto focusing in digital camera. *IEEE Signal Processing Letters*. **16**, pp. 133–136.

Li, Y., Ohmura, I., Takauji, H., Kaneko, S., and Tanaka, T., 2007. Robust focusing by orientation code matching. *ELCVIA*. **7** (3), pp. 752 –758.

Li S. And Yang B., 2008. Multifocus image fusion using region segmentation and spatial frequency. *Image and Vision Computing, Elsevier*. **26**, pp. 971–979.

Mahmood, M., Choi,W.J. and Choi, T. S., 2008. Dct and pca based method for shape from focus. *In Computational Science and Its Applications ICCSA*. **5073**, pp.1025–1034.

Mahmood, M. T., Shim, S. O., and Choi, T. S., 2009. Shape from focus using principal component analysis in discrete wavelet transform. *Optical Engineering*, **48**(5).

Mahmood, M. and Choi, T.S., 2010. Focus measure based on the energy of high-frequency components in the s transform. Opt. Lett. 35(8), pp. 1272–1274.

Malik, A.S. and Choi, T.S., 2007. Consideration of illumination effects and optimization of window size for accurate calculation of depth map for 3D shape recovery. *Pattern Recognition*. **40** (1), pp. 154–170.

Malik, A. S. and Choi, T. S., 2008. A novel algorithm for estimation of depth map using image focus for 3d shape recovery in the presence of noise. *Pattern Recognition.* **41**(7), pp. 2200 – 2225.

Mendapara, P., Minhas, R., and Wu, Q., 2009. Depth map estimation using exponentially decaying focus measure based on susan operator. *Systems, Man and Cybernetics*. pp. 3705-3708.

Meneses, J., Suarez, M. A., Braga, J., and Gharbi, T., 2008. Extended depth of field using shapelet-based image analysis. *Appl. Opt*. **47**(2), pp. 169–178.

Minhas, R., Mohammed, A.A., Wu, Q. M., SidAhmed, M. A., 2009. 3D shape from focus and depth map computation using steerable filters. *Proceedings of the International Conference on Image Analysis and Recognition.* pp.573–583.

Nanda, H. and Cutler, R., 2001. Practical Calibrations for a Real-Time Digital Omnidirectional Camera. *Technical Report, Technical Sketches, Computer Vision and Pattern Recognition*.

Nayar, S. K. and Nakagawa, Y., 1994. Shape from focus. *IEEE Trans. Pattern Anal. Mach. Intell.* **16** (8), pp. 824–831.

Pacheco, P., J., Cristobal, G., Martinez, J. C. and Valdivia, J.F., 2000. Diatom autofocusing in brightfield microscopy: a comparative study. *In Proceedings of the International Conference on Pattern Recognition.* **3**, pp. 314–317.

Pertuz, S., Puig, D. and Garcia, M. A., 2012. Analysis of focus measure operators for shape-from-focus. *Pattern Recognition.* **46** (2013), pp. 1415–1432

Pertuz, S., Puig, D., Garcia, M. A. and Fusiello, A.,2013. Generation of All-in-Focus Images by Noise-Robust Selective Fusion of Limited Depth-of-Field Images. *IEEE Transactions on Image processing.* **22**(3), pp. 1242-1251

Poon, T. C., 1985. Method of two-dimensional bipolar incoherent image processing by acousto-optic two-pupil synthesis. *Opt. Lett*. **10**(5), pp. 197–199.

Santos, A., Solorzano, C.O., Vaquero, J.J., Pena, J.M., Mapica, N. and Pozo, F.D.,1997. Evaluation of auto focus functions in molecular cytogenetic analysis. *Journal of Microscopy*. **188**, pp.264–272.

Shirvaikar, M., 2004. An optimal measure for camera focus and exposure. *Proceedings of the South eastern Symposium on System Theory*. pp. 472–475.

Shen, C. H. and Chen, H., 2006. Robust focus measure for low-contrast images. *Digest of Technical Papers of International Conference on Consumer Electronics*. pp. 69 – 70.

Smith, S. M. and Brady, J. M., 1997. Susan a new approach to low level image processing. *International Journal of Computer Vision*. **23**, pp. 45–78.

Subbarao, M .and Nikzad, A., 1993. Focusing technique. *Image and Signal Processing and Analysis.* **32**(11), pp.2824–2836.

Subbarao, M. and Choi, T., 1995. Accurate recovery of three-dimensional shape from image focus. *IEEE Trans. Pattern Anal. Mach. Intell*. **17(**3), pp. 266–274.

Subbarao, M. and Tyan, J. K., 1998. Selecting the optimal focus measure for autofocusing and depth-from-focus. *IEEE Transactions on Pattern Analysis and Machine Intelligence*. **20**(8), pp. 864 –870.

Stockwell, R., Mansinha, L., and Lowe, R. 1996. Localization of the complex spectrum: the s transform. *Signal Processing, IEEE Transactions*. **44**(4), pp. 998–1001.

Thelen, A., Frey, S., Hirsch, S.and Hering, P., 2009. Improvements in shape from focus for holographic reconstructions with regard to focus operators, neighborhood size, and height value interpolation. *IEEE Transactions on Image Processing.* **18**, pp. 151–157.

Tian, Y., Shieh, K., and Wildsoet, C. F., 2007. Performance of focus measures in the presence of nondefocus aberrations. *J. Opt. Soc. Am. A.* **24**(12), pp. 165–173.

Tian, J. and Chen L.,2010. Multi-focus image fusion using wavelet-domain statistics. *In Proc. IEEE Int. Conf. Image Process*. pp. 1205–1208.

Tsubaki, Y., Kubota, A., Kazuya, K. and Aizawa, K., 2001. All-focused image generation and 3D modeling of microscopic images of insects. *IEEE Proceedings.pp.* 197-200.

Wang, Z., Bovik A. C., Sheikh, H.R. and Simoncelli, E. P., 2004. Image quality assessment: From error visibility to structural similarity. *IEEE Trans. Image Processing*. **13(**4), pp. 600–612.

Wee, C. and Paramesran, R., 2007. Measure of image sharpness using eigenvalues. *Information Sciences*. **177**, pp. 2533–2552.

Xiong, Y. and Shafer, S. A., 1994. Variable window gabor filters and their use in focus and correspondence. *In Proc. of IEEE Conf. on Computer Vision and Pattern Recognition*. pp. 668–671.

Xiong, Y. and Shafer, S., 1997. Moment and hypergeometric filters for high precision computation of focus, stereo and optical flow. *International Journal of Computer Vision*. **22**(1), pp. 25–59.

Yang, G. and Nelson, B., 2003. Wavelet-based autofocusing and unsupervised segmentation of microscopic images. *Proceedings of the IEEE/ RSJ International Conference on Intelligent Robots and Systems.* **3**, pp. 2143 – 2148.

Yap, P. and Raveendran, P., 2004. Image focus measure based on Chebyshev moments. *IEEE Proceedings-Vision, Image and Signal Processing*. **151**, pp.128–136.

Zhang, Z. and Blum, R.,1999. A categorization of multiscale-decompositionbased image fusion schemes with a performance study for a digital camera application. *Proc. IEEE*. **87(**8), pp. 1315–1326.

Zhang, Y., Zhang, Y., and Wen, C., 2000. A new focus measure method using moments. *Image and Vision Computing*. **18**(12), pp.959 – 965.

Other Sources

Aydin, T., (2011). Cifte ag metoduyla stereo, odak ve bulanıklık bilgisini kullanarak resimlerden derinlik çıkarımı.PhD thesis. İzmit, Gebze Teknik Universitesi

Krotkov, E. P., (1987). Exploratory Visual Sensing for Determining Spatial Layout with an Agile Stereo Camera System. PhD thesis. Philadelphia, University of Pennsylvania.

Tenenbaum, J. M., (1971). Accommodation in computer vision. PhD thesis. Stanford, Stanford University Stanford.